J Mater Sci (2021) 56:2748–2762

Polymers & biopolymers

Effects of the curing atmosphere on the structures and properties of polybenzoxazine films

Shuai Zhang[1,2], Qichao Ran[1,*], Xiaokun Zhang[2], and Yi Gu[1]

[1] College of Polymer Science and Engineering, State Key Laboratory of Polymer Materials Engineering, Sichuan University, Chengdu 610065, China

[2] State Key Laboratory of Electronic Thin Films & Integrated Devices, School of Energy Science and Engineering, University of Electronic Science and Technology of China, 2006 Xiyuan Avenue, West High-Tech Zone, Chengdu 611731, Sichuan, China

Received: 23 July 2020
Accepted: 2 October 2020
Published online: 19 October 2020

ABSTRACT

The effects of four different curing atmospheres, i.e., static air, circulating air, nitrogen and vacuum, on the polymerization mechanism, chemical structure, hydrogen bonding, mechanical property, thermal property, water contact angle, etc., of the polybenzoxazine films were systematically studied. It was found that curing in air caused more oxidation and decomposition, generating more benzoquinones, carbonyl groups and iminium ions in the resultant polybenzoxazine films. Consequently, the films cured in air were less cross-linked, darker in color and more brittle. The films cured in static air (SA) showed tensile strength and elongation at break of 12.59 MPa and 2.16%, respectively, which were 61.24 MPa and 2.74% lower than those of the films cured in nitrogen (N2). Moreover, it was demonstrated that more intramolecular rigid –OH···N hydrogen bonding was formed in the films cured in air, which was believed to be the fundamental reason for the lower chemical cross-linking density and poorer toughness. Nevertheless, these films showed higher char yield due to the formation of more thermally stable groups in oxidation process. Further investigation on chemical structures, hydrogen bonding and water contact angles of the upper and lower surfaces of the films revealed that the upper surfaces were more inclined to be oxidized and decomposed during curing and more intramolecular hydrogen bonding (–OH···N HB) was formed on upper surfaces, which led to increased water contact angles.

Handling Editor: Gregory Rutledge.

Address correspondence to E-mail: ranqichao@scu.edu.cn

https://doi.org/10.1007/s10853-020-05425-5

GRAPHIC ABSTRACT

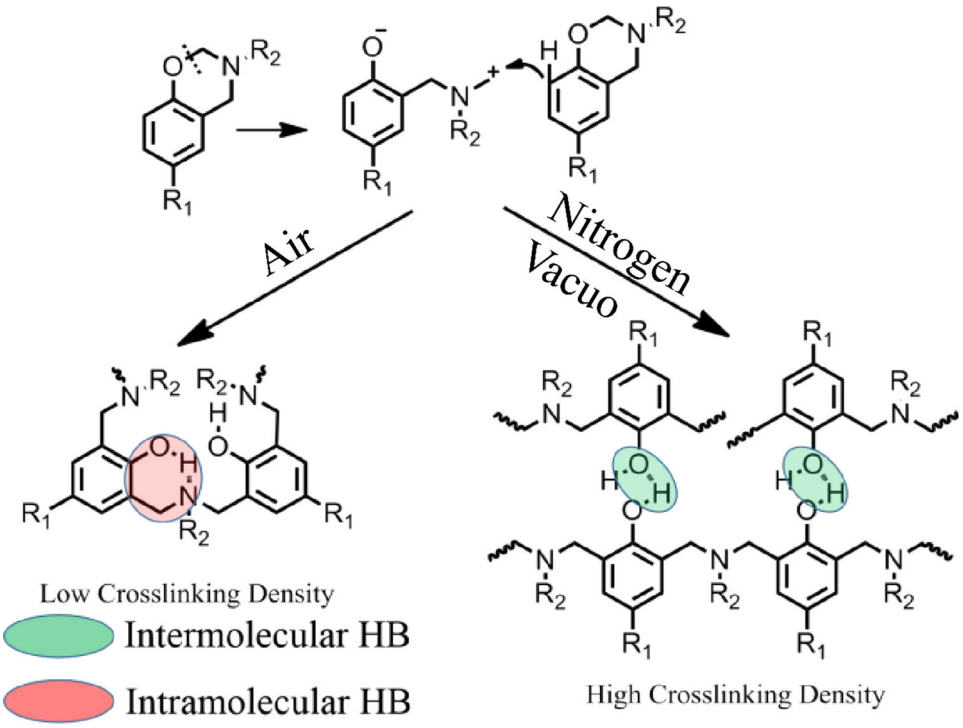

Introduction

Polybenzoxazines that can be formed by ring-opening polymerization (ROP) of nitrogen and oxygen containing six-membered heterocyclic compounds have drawn much attention and research interest from industrial and academic communities, especially in recent 30 years [1–11]. Polybenzoxazines are versatile resins which meet a variety of application scenarios. Firstly, their high T_gs, high strength, high modulus and good thermal stability ensure their application in harsh environments like aeronautics and astronautics [12–15]. Secondly, their good dielectric properties, dimensional stability, flame retardance and low water uptake make them good candidates for electronic devices [16–21]. Moreover, the tremendous design flexibility is of great potential to develop functional application such as shape memory, self-healing, pollution treatment, super capacitor, CO_2 absorption, etc., based on polybenzoxazines [22–28]. Additionally, polybenzoxazines cater to the concept of green chemistry and sustainable development since many benzoxazine monomers can be synthesized from bio-based compounds [13, 29–32]. It is also noteworthy that their outstanding processability makes them suitable for multiple process techniques such as coating, casting, resin transfer molding and hot-pressing [33–36].

ROP of benzoxazine monomers is a complex process and can generate polybenzoxazines with distinct chemical structures and properties. Generally, ROP of benzoxazine firstly involves cleavage of C–O bonds in the oxazine ring and formation of phenoxy anions and carbocations. Then the electrophilic carbocations are able to attack the electronegative sites such as nitrogen and oxygen atoms in other oxazine rings, ortho-position of phenolic moieties or phenyl rings of aromatic amines to produce N,O-acetal structures, phenolic Mannich structures and arylamine Mannich structures, respectively. Due to the huge differences of chemical structures, the properties of the polybenzoxazines can be tuned in a great

range. Many works have been done to understand the polymerization mechanism and control the chemical structures and properties of the polybenzoxazines, either by selection of catalysts, solvents and polymerization temperature or monomer design [37–42]. It is demonstrated by Ishida, Chao, et. al. that N,O-acetal structures are thermally unstable and they exist at relatively lower temperature; otherwise they will transform to phenolic Mannich structures at higher temperature [42–44]. Our team recently proves that arylamine Mannich polybenzoxazines are tougher and possess higher cross-linking density with more intermolecular hydrogen bonding formed and more aromatic amine moieties linked into the backbone [45, 46]. In most cases, however, the polybenzoxazines are mainly composed of phenolic Mannich structures since no catalysts and solvents are used and high curing temperature is needed to obtain necessary mechanical strength and thermal properties. It should be noted that the distinguished properties that have been emphasized frequently are mostly attributed to the phenolic Mannich polybenzoxazines [3, 47, 48]. Though they possess many advantages, one of the serious drawbacks accompanying the phenolic Mannich polybenzoxazines is the brittleness, which is seriously hindering the exploitation and wider application of polybenzoxazines. According to the previous reports, the poor toughness is believed to be the consequence of low cross-linking density and formation of massive rigid intramolecular hydrogen bonding [49–52]. To address this issue, some studies introduce extra hydrogen bonding donors and/or acceptors to form more hydrogen bonding that strengthens molecular interactions. Moreover, the additional hydrogen bonding disrupts the rigid intramolecular hydrogen bonding, which increases the molecular weight and the cross-linking density [53–55]. Some other studies increase the cross-linking densities of polybenzoxazines by simply copolymerizing with other resins such as epoxy resins and cyanate esters [56–59]. Though many methods have been established to improve the cross-linking densities and the brittleness of polybenzoxazines, few reports have tried to understand the relationship between curing conditions and structures and properties of the polybenzoxazines, let alone tailor the structures and properties accordingly [60]. Hence, it would be very meaningful to reveal the internal correlations so that improvements in performances can be realized by varying the curing conditions in practical application.

The purpose of this work was to elucidate the effects of curing atmospheres on the structures and properties of the polybenzoxazines. Four curing atmospheres including static air, circulating air, nitrogen and vacuum were chosen as variables. A typical benzoxazine monomer 2,2-bis(4-phenyl-3,4-dihydro-2H-1,3-benzoxazinyl)-isopropane (BA-a) was selected as object of investigation and films were made to maximally reflect the influences of curing atmospheres. The difference of polymerization mechanism, chemical structure, hydrogen bonding, mechanical property, thermal property and water contact angle were systematically studied. The correlations between curing atmospheres, structures and properties revealed in this work are believed to further our understanding of the ROP mechanism and guide the practical applications of polybenzoxazines.

Experimental

Materials

Analytical grade *N*,*N*-dimethylformamide (DMF) was purchased from Chengdu Kelong Chemical Reagents Co., Ltd (Chengdu China) and used as received. Highly pure BA-a was synthesized in our laboratory following the reported procedure [1, 60, 61].

Preparation of polybenzoxazine films in different atmosphere

Crystalline BA-a was dissolved in DMF to give light yellow and transparent solutions with a resin content of 30 wt% in vials. The solutions were then coated onto horizontally placed glass slides in a vacuum oven, followed by evaporating the organic solvent in high vacuum (− 0.09 MPa) at 80 °C and 100 °C for 2 h, respectively. For films cured in static air, the air valve was gently opened to allow slow inflation of air and reached standard atmospheric pressure. For films cured in nitrogen, the oven was slowly filled with high-purity nitrogen through the valve and reached standard atmospheric pressure. For films cured in vacuum, the constant pressure of − 0.09 MPa was kept throughout the whole curing process. For films cured in circulating air, the films

formed after evaporation of organic solvent were transferred to a pre-heated air circulating oven. Thereafter, the films were cured at 120 °C, 140 °C, 160 °C, 180 °C and 200 °C for 2 h, respectively. Due to the fact that polybenzoxazine films will shrink and fracture along with the glass slides if they were naturally cooled to room temperature, the films were immersed in boiling water to obtain integral films. After exfoliation from the glass slides, the films were dried in air circulating oven at 100 °C for 2 h. The films cured in static air, circulating air, vacuum and nitrogen were labeled as SA, CA, VA and N2, respectively. It should be noted that the temperature of the vacuum oven and the air circulating oven is accurately calibrated before curing, and the other curing conditions such as curing time, immersing time and drying process were also deliberately controlled to reduce the experimental error.

Characterization

Differential scanning calorimetry (DSC) tests were conducted by a DSC Q20 (TA Instruments) at a heating rate of 10 °C/min under nitrogen atmosphere. Calibration was made using an indium standard; about 3 mg of samples was sealed in the aluminum pan for scanning. Fourier transform infrared (FTIR) spectra and attenuated total reflection infrared (ATR-IR) spectra were obtained with a Nicolet-560 spectrometer in the range of 4000–400 cm^{-1} at a resolution of 4 cm^{-1}. For powder samples that were ground from polybenzoxazine films, the powder samples were mixed with spectroscopy grade KBr to make pellets and the spectra reflected the holistic chemical structures, while the films were subjected to the ATR-IR spectroscopy to probe the chemical structures of the upper or lower surfaces. To clarify hydrogen bonding distribution, the heavily overlapped bands in the hydroxyl absorption region of FTIR spectrum from 3800 to 1700 cm^{-1} were curve-resolved using a mixed Lorentzian–Gaussian function in NICOLET OMNIC software. It was calculated until the least-squares curve-fitting converged. The UV–Vis absorption spectra were recorded on a UV3600 (Shimadzu Corporation) using polybenzoxazine films in the range of 450–800 nm. Tensile tests were conducted with an INSTRON 5967 universal testing machine following the ASTM D882 at a crosshead velocity of 2 mm/min at 25 °C. The dimensions of the samples were around 4 cm × 1 cm × 0.02 cm, and the reported data were average of at least five tests. The fracture surfaces of the films were observed using a Philips XL-30 FEG scanning electron microscopy (SEM). All samples were coated with an ultra-thin electrically conducting gold by high vacuum evaporation. Dynamic mechanical analysis (DMA) measurements were taken on a DMA Q800 dynamic mechanical analyzer (TA Instruments) with a frequency of 1 Hz and a heating rate of 5 °C/min, from 40 °C to 260 °C in air atmosphere. The dimension of the samples was around 3 cm × 1 cm × 0.02 cm. Thermal gravimetric analysis (TGA) was performed on NETZSCH TG 209F1 Iris (NETZSCH Instruments); the polymer samples were heated from 35 to 800 °C in nitrogen atmosphere with a flow rate of 40 mL/min and a heating rate of 10 °C/min. For thermostatic curing weight loss tests, the BA-a monomer was ramped from 35 °C to 190 °C at a heating rate of 10 °C/min and then kept at 190 °C for 60 min in nitrogen and air, respectively, with gas flow rate of 40 mL/min. The water contact angles of the films were measured at 25 °C with a Kruss DSA25 goniometer (Kruss Scientific Instruments) interfaced with image-capture software by injecting a 4-μL deionized water drop.

Results and discussions

Chemical structures and hydrogen bonding analysis of polybenzoxazine films

Prior to discussing the structures and properties of the polybenzoxazine films, it should be pointed out that all films possessed similar curing degree, as suggested by the very similar residual enthalpy (Figure S1). Therefore, the following comparisons and discussions are reasonable. In appearance, the polybenzoxazine films cured at different atmospheres showed obvious color difference, that is, the films cured in air (SA and CA) were darker than VA and N2. As shown in Figure S2, SA and CA were reddish brown, while VA and N2 were light yellow and more transparent. In order to illuminate experimentally, the UV–Vis transmission spectra of the films were obtained and are presented in Fig. 1. It is evident that the spectra can be divided into two categories, the spectra of SA and CA were almost identical and showed much lower transmittance than N2 and VA in the range of 525–800 nm, which was

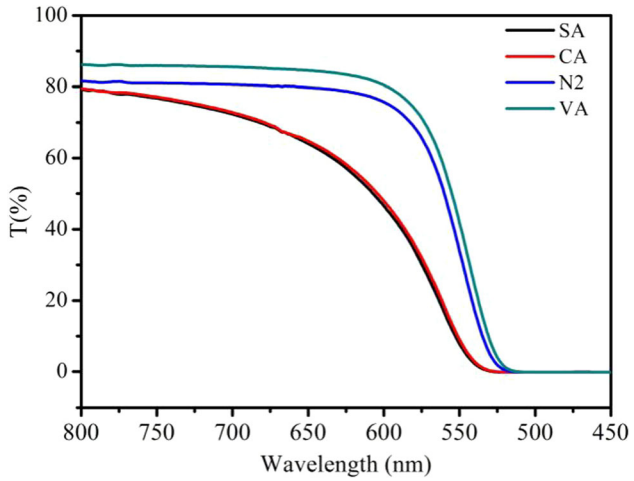

Figure 1 UV–Vis transmission spectra of SA, CA, N2 and VA in the range of 450–800 nm.

the reason why SA and CA were darker than N2 and VA. For the transparent film, the color of the film is the transmitted color that one can see. The most transmitted color (> 50%) of SA and CA was in the range of 600–800 nm, which covers to the range of red (622–770 nm) and orange (597–622 nm) color; hence SA and CA showed reddish brown color. Comparatively, N2 and VA showed high transmittance in the range of 550–800 nm (> 50%), which covers the range of yellow (577–597 nm) color, as a result, N2 and VA were light yellow. Many research papers have mentioned that polybenzoxazines show dark color. Typically, polybenzoxazines without extra functional groups are wine red while polybenzoxazines with extra functional groups are black and totally opaque [23, 62, 63]. Some explained that oxidation will deepen the color and some claimed that higher cross-linking density would cause dark color. In this work, the darker color of SA and CA was demonstrated to be caused by the oxidation of phenolic moieties rather than higher cross-linking density because SA and CA possessed lower cross-linking density, which will be discussed later.

The FTIR spectra of BA-a, SA, CA, N2 and VA are shown in Fig. 2. For all samples, the most characteristic absorption band of oxazine ring at 947 cm^{-1} and 1233 cm^{-1} (C–O–C stretching) disappeared completely, and a broad absorption band of hydroxyl group showed at around 3400 cm^{-1}, which suggested the ROP of BA-a and formation of massive phenolic hydroxyls. Moreover, the characteristic absorption peaks of tri-substituted benzene ring at 822 cm^{-1} (Ar–H stretching) and 1498 cm^{-1} (C=C stretching) disappeared, and tetra-substituted benzene ring absorption peak emerged at 1481 cm^{-1} and 1487 cm^{-1} (C=C stretching). Additionally, a new and intense absorption band at 1171 cm^{-1} that was ascribed to C–N–C stretching appeared. These features demonstrated that all films were mainly consisted of phenolic Mannich bridge structures. Though the spectra of SA, CA, N2 and VA shared so much in common, they can still be divided into two groups according to some minor differences. According to the nuances, the spectra of SA and CA can be classified as one group while those of N2 and VA as another. Specifically, in the spectra of SA and CA, the absorption bands at 1652 cm^{-1} and 1680 cm^{-1} (black arrow) were higher than those of N2 and VA. According to the previous reports, these bands are

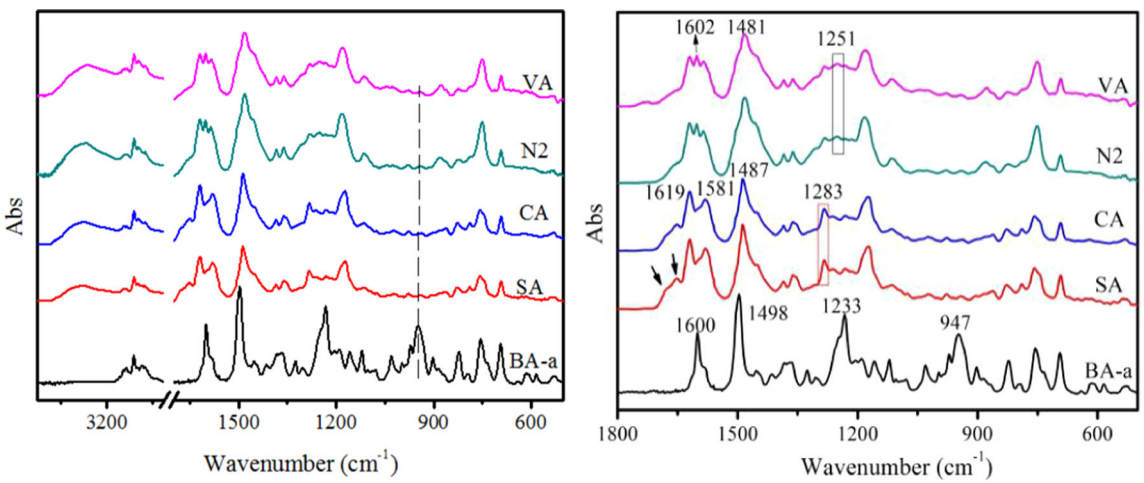

Figure 2 FTIR spectra of BA-a, SA, CA, N2 and VA.

attributed to benzoquinone groups and iminium ions [45, 48]. Moreover, the weight loss during the curing process in air and nitrogen was monitored by TGA (Figure S3). As can be seen in Figure S3, air caused more weight loss (2 wt%) during thermostatic in 60 min than nitrogen atmosphere. As the curing time prolonged, more weight loss may be caused. Hence, as is shown in Scheme 1, it is deduced that curing in air would cause oxidation of phenolic groups and more decomposition of thermally unstable moieties, forming more benzoquinone groups (structure 1) and iminium ions (structure 5), and benzoquinone groups are responsible for the darker color of SA and CA.

In addition to the benzoquinone groups and iminium ions, the absorption band of Ar–O bonds in phenolic hydroxyls was different between the two groups. The Ar–O absorption band of SA and CA was at around 1283 cm^{-1} while the peak of Ar–O absorption showed up at around 1251 cm^{-1} for N2 and VA, which was speculated to be resulted from the variation of the hydrogen bonding composition, that is, the Ar–O absorption band showed up at around 1283 cm^{-1} if more intramolecular (–OH···N and –O···H^+N^-) hydrogen bonding was formed and at around 1251 cm^{-1} when more intermolecular (–OH···O and –OH···π) hydrogen bonding was formed. Such feature is more evident in the spectra of arylamine Mannich polybenzoxazines where much more intermolecular hydrogen bonding is formed (Figure S4). To manifest this theory, the FTIR spectra in the hydroxyl groups absorption region (3800–1700 cm^{-1}) of CA and N2 were curve-fitted using a mixed Lorentzian-Gaussian function and the results are given in Fig. 3 and Table 1. For simplification, the absorption band of C–H at around 2900 cm^{-1} is not shown. As expected, the content of intramolecular hydrogen bonding in CA was around 10% higher than that of N2, and more intermolecular –OH···O and -OH···π hydrogen bonding was formed in N2. Therefore, it can be concluded that polybenzoxazine cured in air atmosphere would form more rigid intramolecular –OH···N hydrogen bonding.

Tensile property of polybenzoxazine films

To investigate the differences of mechanical properties brought by curing atmosphere, the films were subjected to tensile tests. Figure 4 presents the stress–strain curves of SA, CA, N2 and VA, Table 2 summarizes the data from tensile tests. Clearly, the tensile strength, tensile modulus and elongation at break of SA and CA were much lower than those of N2 and VA. The tensile strength of SA and CA were 12.59 MPa and 14.76 MPa, respectively, while that of N2 reached 73.83 MPa, which was almost 5 times higher. Additionally, the elongation at break of N2 was twice as much as SA and CA. Apparently, these characteristics proved that N2 and VA were stronger and tougher than SA and CA. According to the previous structural analysis, the oxidation, decomposition of polybenzoxazine during curing and formation of more rigid intramolecular –OH···N hydrogen bonding may be the main cause. Additionally, the higher chemical cross-linking density to be discussed later was another important reason. Regarding the rough and curvy stress–strain curves of SA and CA, it should be noted that these films were so brittle that they fractured during the testing process, so the clamping force of SA and CA was reduced when compared with N2 and VA. Consequently, the tensile properties of SA and CA may not be accurate.

After tensile tests, the fracture surfaces of the films were observed by SEM and the images are shown in Fig. 5. The cross sections of SA and CA were very flat

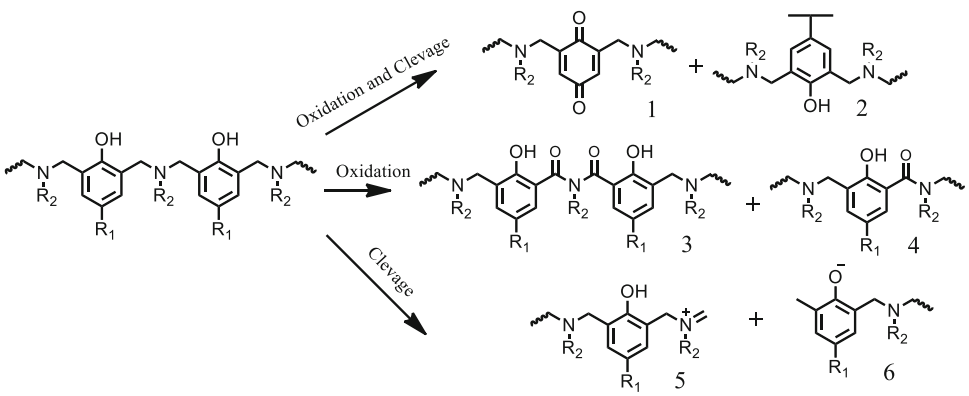

Scheme 1 Possible oxidation and decomposition process of polybenzoxazine cured in air.

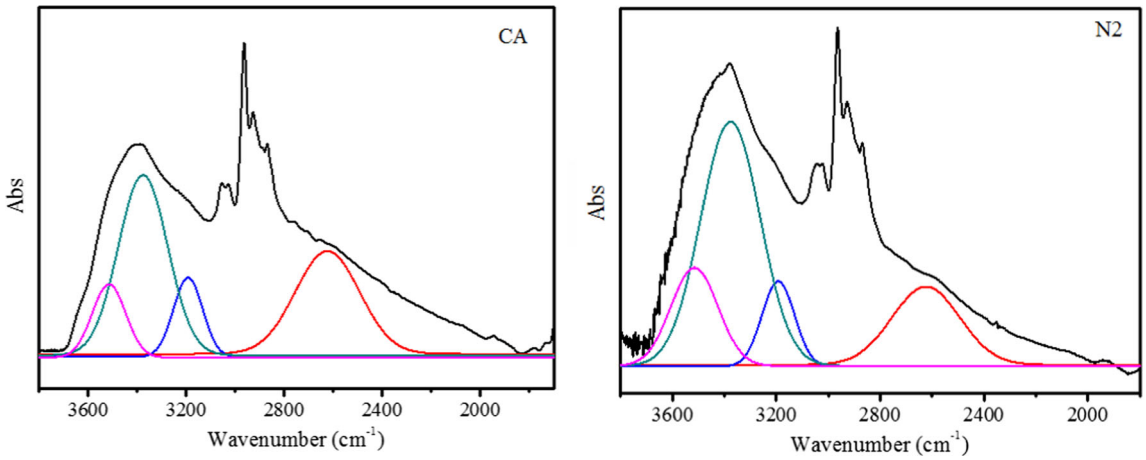

Figure 3 Curve fitting results of CA and N2 in the range of 3800–1700 cm^{-1}.

Table 1 Hydrogen bonding distributions of CA and N2 from curve fitting of FTIR spectra in the range of 3800–1700 cm^{-1}

Sample	–O···H^+N^- (%)	–OH···N (%)	–OH···O (%)	–OH···π (%)	Intra-HB (%)
CA	29.2	12.8	39.8	18.1	42.0
N2	17.3	14.8	48.1	19.8	32.1

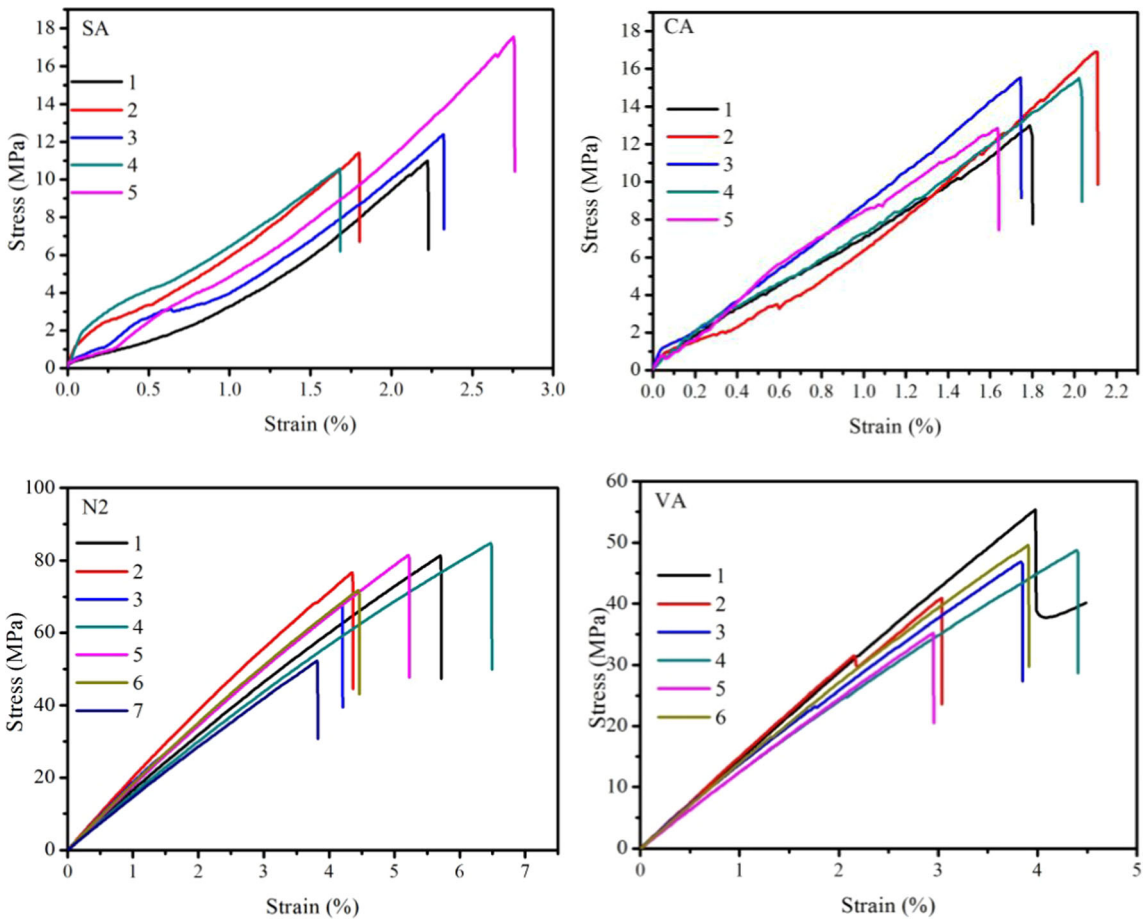

Figure 4 Stress–strain curves of SA, CA, N2 and VA.

Table 2 Data from tensile tests of SA, CA, N2 and VA

Sample	Tensile strength (MPa)	Tensile modulus (GPa)	Elongation at break (%)
SA	12.59 ± 2.86	0.92 ± 0.61	2.16 ± 0.43
CA	14.76 ± 1.76	0.90 ± 0.13	1.87 ± 0.20
N2	73.83 ± 11.15	1.79 ± 0.19	4.90 ± 0.95
VA	46.14 ± 7.08	1.41 ± 0.11	3.78 ± 0.66

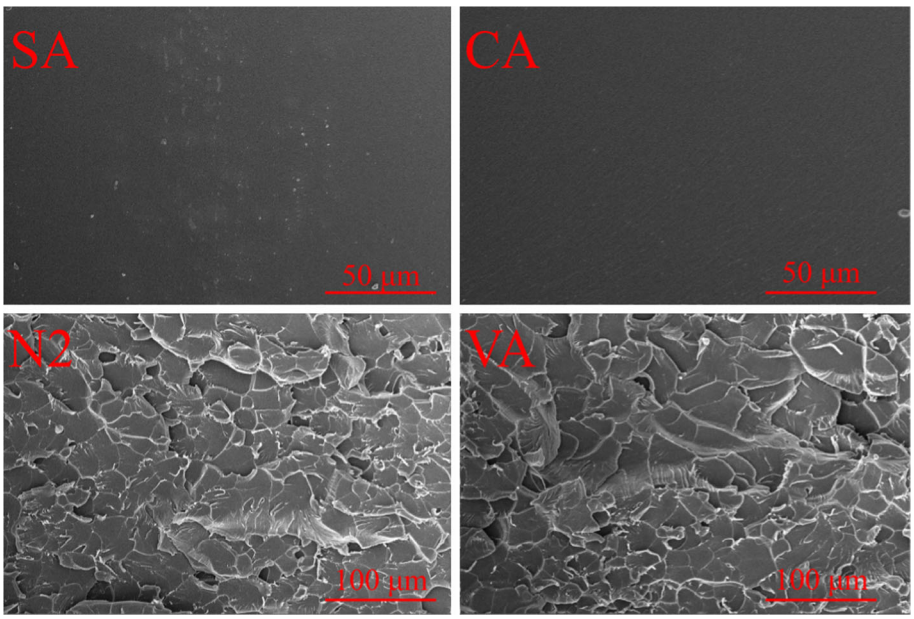

Figure 5 Fracture surfaces of SA, CA, N2 and VA.

and smooth, which were typical features of brittle fracture. On the contrary, the cross sections of N2 and VA were full of fish-scale patterns, showing the characteristics of ductile fracture. Though the stress–strain curves of N2 and VA indicated that brittle fracture happened, the morphology of the fracture surfaces further demonstrated the better toughness and flexibility of N2 and VA than the films cured in air.

Thermal properties and cross-linking densities of polybenzoxazine films

The films were subjected to dynamic mechanical analysis tests and the diagrams and key data are shown in Fig. 6 and Table 3. The storage modulus at glassy state of the four samples showed no obvious patterns, though VA was somewhat exceptional. However, the storage modulus at rubbery state of the films cured in air was clearly lower than N2 and VA (Fig. 6b). The storage modulus of CA at $T_{g\ tan}$ + 40 K was just 4.4 MPa while that of N2 was 20.0 MPa, which was almost 4 times higher. At rubbery state, physical interaction such as hydrogen bonding is negligible and the modulus is mainly retained by chemical cross-linking. So, the cross-linking densities of SA and CA are supposed to be lower than those of N2 and VA. Furthermore, the cross-linking density ρ was calculated by equation of rubbery elasticity $\rho = E'/3\Phi RT$ [64–66], where Φ is the front factor, which is assumed to be 1, T is the absolute temperature, R is the gas constant, and E' is the storage modulus at temperature $T_{g\ tan}$ + 40 K. As listed in Table 3, the chemical cross-linking density of CA was the lowest (0.37×10^3 mol/m^3) and that of N2 was the highest (1.67×10^3 mol/m^3). Clearly, due to the circulating air during curing process, the polymer chains of CA were oxidized and decomposed the most thoroughly, thus leading to the lowest chemical cross-linking density. This was also the reason why CA showed the worst mechanical property. In addition to the lower chemical cross-linking density, the thermal resistance was also affected. When comparing the glass transition temperature determined by peak temperature of loss modulus diagram ($T_{g\ E''}$), the $T_{g\ E''}$s of SA and CA were lower than those of N2 and VA, which is in

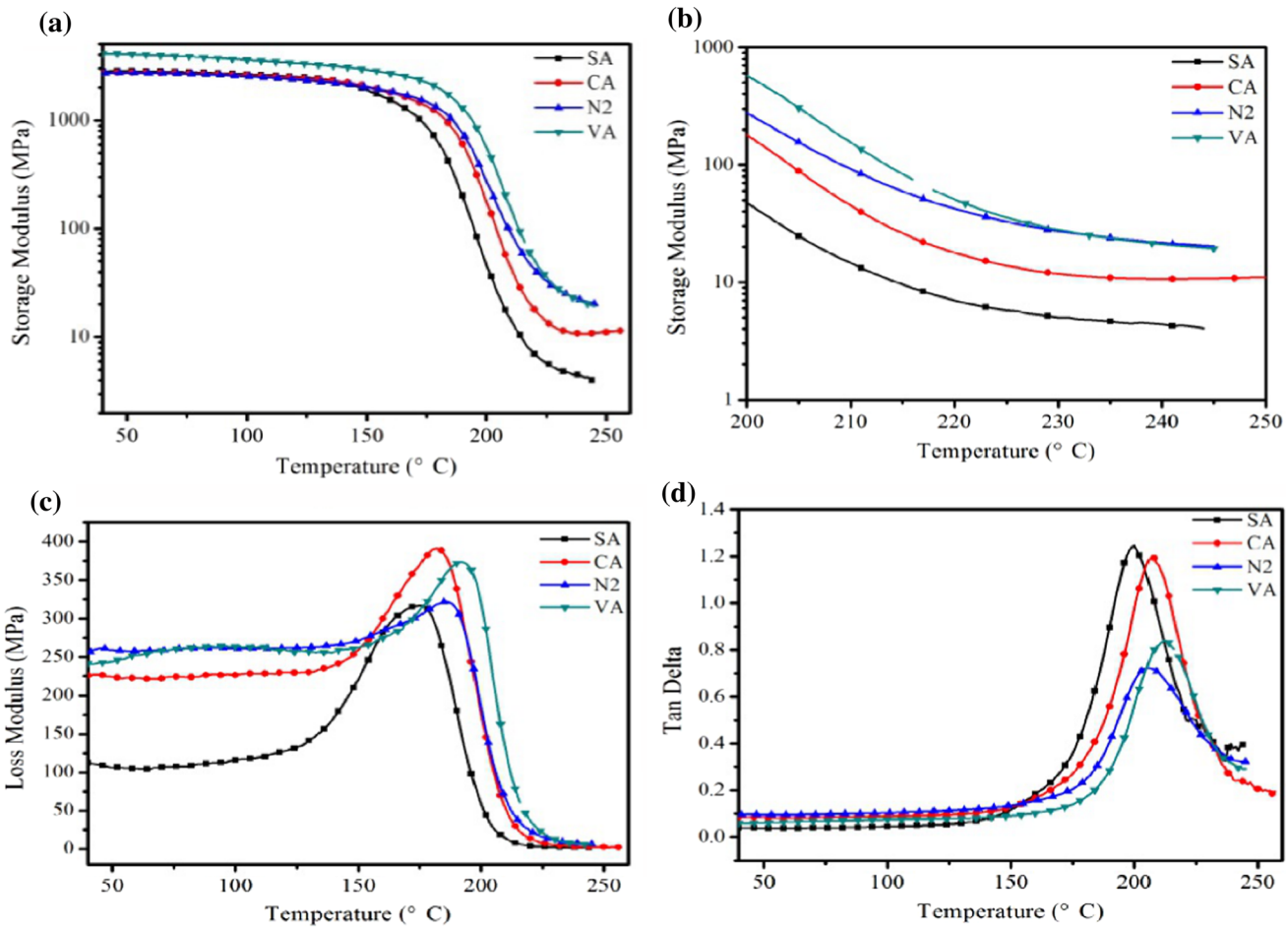

Figure 6 DMA diagrams of SA, CA, N2 and VA, **a** storage modulus, **b** storage modulus at rubbery state, **c** loss modulus, **d** tangent delta.

Table 3 Summary of DMA, DSC data and calculated cross-linking densities

Sample	E' (MPa, 40 °C)	$T_{g\ DSC}$ (°C)	$T_{g\ E''}$ (°C)	$T_{g\ tan\delta}$ (°C)	E' (MPa, $T_{g\ tan}$ + 40 K)	ρ (mol/m^3)
SA	2809	152.6	175.8	199.8	10.9	0.91×10^3
CA	2705	160.1	182.3	207.7	4.4	0.37×10^3
N2	2675	168.7	185.6	205.9	20.0	1.67×10^3
VA	4123	164.0	193.1	212.2	17.3	1.43×10^3

accordance with the DSC test results. SA showed the lowest $T_{g\ E''}$ of 175.8 °C and VA showed the highest $T_{g\ E''}$ of 193.1 °C. Such difference proved that curing in air was disadvantageous for higher thermal resistance as well. It was worth noting that the peak of tangent delta diagram (Fig. 6d) showed obvious differences between the air-cured systems and non-air-cured systems, that is, the peaks of SA and CA were higher and sharper than those of N2 and VA. Here the polybenzoxazine films were homogeneous and unitary; hence the tangent delta peak reflected the polymer chain relaxation process during elevating temperature. The high and sharp tangent delta peaks of SA and CA indicated fast relaxation because they possessed very low cross-linking density and less intermolecular interaction.

As for the reason why N2 and VA possessed higher chemical cross-linking density, it was believed to be a result of more intermolecular hydrogen bonding in addition to less decomposition during curing. When

cured in air, the oxidation and decomposition caused lower cross-linking density and shorter polymer chain; thus the polymer chain was less constrained and more flexible. Furthermore, the higher moveability led to the formation of more intramolecular rigid –OH···N hydrogen bonding. As is demonstrated by Po Yang and Suwabun Chirachanchai et. al.[67–69], –OH···N hydrogen bonding impeded chain propagation of polybenzoxazine, therefore, leading to short polymer chain and low cross-linking density. On the contrary, when cured in inert nitrogen or in vacuum where less or no oxidation and decomposition happened, more intermolecular –OH···O hydrogen bonding was formed. Consequently, the polymer chains were more stretched and cross-linking densities were higher. According to the above discussion, the proposed relationship between curing atmosphere, hydrogen bonding and cross-linking density is illustrated in Scheme 2.

The thermal stability of the films cured in different atmospheres was also evaluated, and the results are shown in Fig. 7 and Table 4. Interestingly, SA and CA showed lower initial decomposition temperature (T_{d5} and T_{d10}) but higher char yield (Y_c) at 800 °C than N2 and VA. Specifically, the T_{d5} of SA (300.0 °C) was the lowest while that of VA (325.4 °C) was the highest. As for the Y_c at 800 °C, the lowest was assigned to N2 (38.6%) while the highest was attributed to CA (48.7%). Such data seemed to be contradictory, but they can be well explained by the conclusions obtained previously. Firstly, SA and CA contained more iminium ions that were thermally unstable and liable to decompose. Secondly, lower cross-linking densities were detrimental to T_{d5} because more chain ends were formed in SA and CA. Specifically, the small shoulder peak in the DTG curve of SA in the range of 250–350 °C corresponded to the decomposition of iminium ions and loose chain ends. However, in the temperature range where the backbone C–N–C bonds in the phenolic Mannich bridge structures began to decompose (~ 400 °C), the function of high cross-linking density was not as important. As suggested in Scheme 1, the oxidation process would generate more benzoquinone (structure 1), amide (structure 4) and even imide (structure 3) groups in SA and CA. These groups were supposed to be much stronger than the C–N–C bonds in the phenolic Mannich bridge structures; therefore the decomposition rate of SA and CA in the temperature range of 350–500 °C was much lower than that of N2 and VA, as shown in the DTG curves. As a consequence of these factors combined, SA and CA showed lower T_{d5} but higher Y_c.

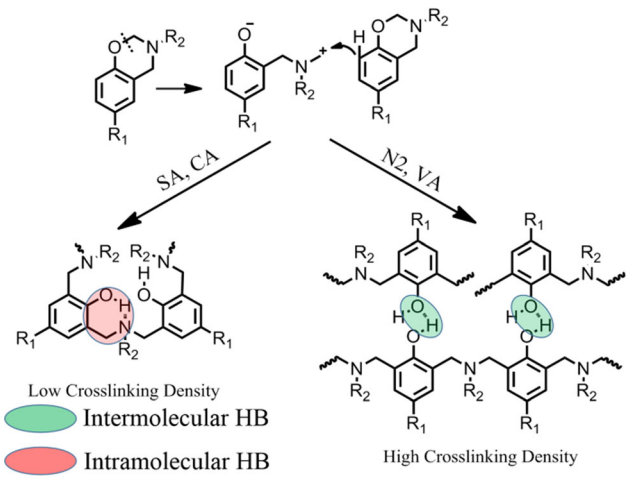

Scheme 2 Relationship between curing atmosphere, hydrogen bonding and cross-linking density.

Structural analysis and water contact angles of the surfaces of the polybenzoxazine films

The chemical structures and hydrogen bonding distribution of the two surfaces of the films are of great interest because they could reveal more information about curing in different atmospheres and determine some surface properties such as water contact angles. The ATR-IR spectra of upper and lower surfaces of the films are shown in Fig. 8 and Figure S5. Here the ATR-IR spectra of the upper surface of CA were denoted as CA-up while the lower surface was denoted as CA-down, and the others were named with the same manner. For the two surfaces of CA, their ATR-IR spectra were generally identical except for the two bands at 1679 cm^{-1} and 1650 cm^{-1} that were assigned to iminium ions and benzoquinone structures. The intensities of the two bands in CA-up were much higher than those of CA-down, which suggested that the upper surface of CA was oxidized and decomposed more heavily. Similar feature was also observed in the ATR-IR spectra of the surfaces of SA, N2 and VA, which meant that upper surfaces were more inclined to decompose than the lower surfaces. However, the intensities of the two bands in N2 and VA were much lower than the air-cured samples, and the two bands can hardly be noticed in the ATR-IR spectra of N2-down and VA-down,

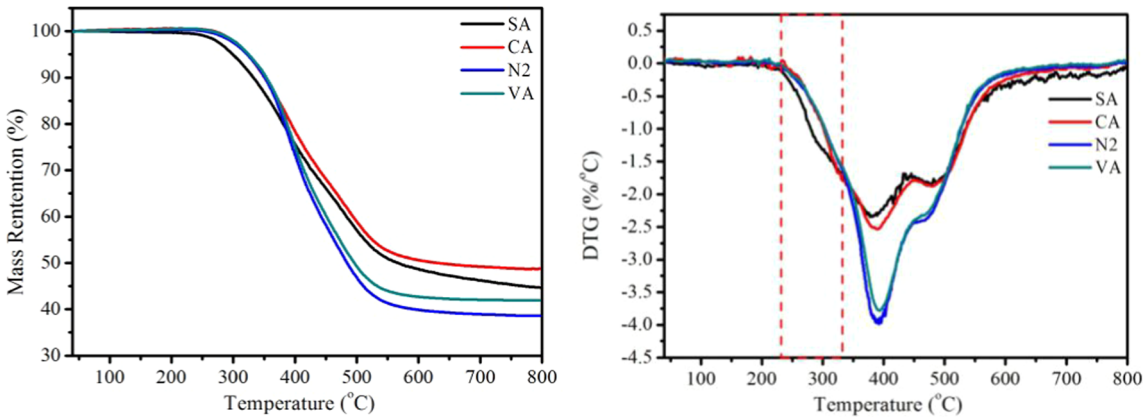

Figure 7 TGA and DTG thermograms of SA, CA, N2 and VA.

Table 4 Summary of TGA data of SA, CA, N2 and VA

Sample	T_{d5} (°C)	T_{d10} (°C)	Y_c at 800 °C (%)
SA	300.0	332.2	44.7
CA	323.3	351.3	48.7
N2	322.3	351.3	38.6
VA	325.4	354.4	42.0

which indicated that nearly no oxidation or decomposition happened in the lower surfaces of N2 and VA. Interestingly, the intensity of the mono-substituted benzene ring absorption band at around 743 cm^{-1} was higher in N2-down and VA-down than it was in other spectra, meaning less aromatic amines were decomposed, which further supported the above statement.

The hydrogen bonding distributions of the surfaces of the polybenzoxazine films were also investigated by curve fitting of the ATR-IR spectra in the hydroxyl absorption range (3800–1700 cm^{-1}), and the data are shown in Table 5. It was obvious that more intramolecular hydrogen bonding (–OH···N and –O···H^+N^-) was formed in the upper surfaces than it was in the lower surfaces. The difference of intramolecular hydrogen bonding content between the two surfaces in CA was very small (0.1%) while that of VA was the biggest (6.0%). A probable cause for such phenomenon may be that the high mobility of circulating air ensured homogeneity of CA films and the upper and lower surfaces shared similar chemical structures and hydrogen bonding distributions.

It is well known that the surface energy and contact angles of polybenzoxazines are closely related to the hydrogen bonding distributions [70–72]. Specifically, intramolecular hydrogen bonding is less polar and beneficial for lower surface energy while intermolecular hydrogen bonding is more polar and responsible for high surface energy. The water contact angles (WCAs) of upper and lower surfaces of polybenzoxazine films were measured, the profiles are shown in Figure S6 and the data are listed in Table 6. Obviously, the WCAs of upper surfaces were higher than those of the lower surfaces. Moreover, the differences between the WCAs are positively correlated to the differences between the intramolecular hydrogen bonding contents. For example, the difference of WCA between the two surfaces in CA was the smallest (1.3°) while that of VA was the biggest (8.9°). In conclusion, higher content of intramolecular hydrogen bonding led to smaller WCA, which was in accordance with the previous findings. It should be noted that the absolute values of WCAs between different films were not very much comparable because of the different chemical structures.

Conclusions

After systematic study of the effects of curing atmospheres on the structures and properties of the polybenzoxazine films, it was found that curing in air could lead to more oxidation, more decomposition, formation of more thermally unstable iminium ions, more light-absorbing benzoquinone groups, more thermally stable imine analogues, decreased cross-linking density and more rigid intramolecular (–

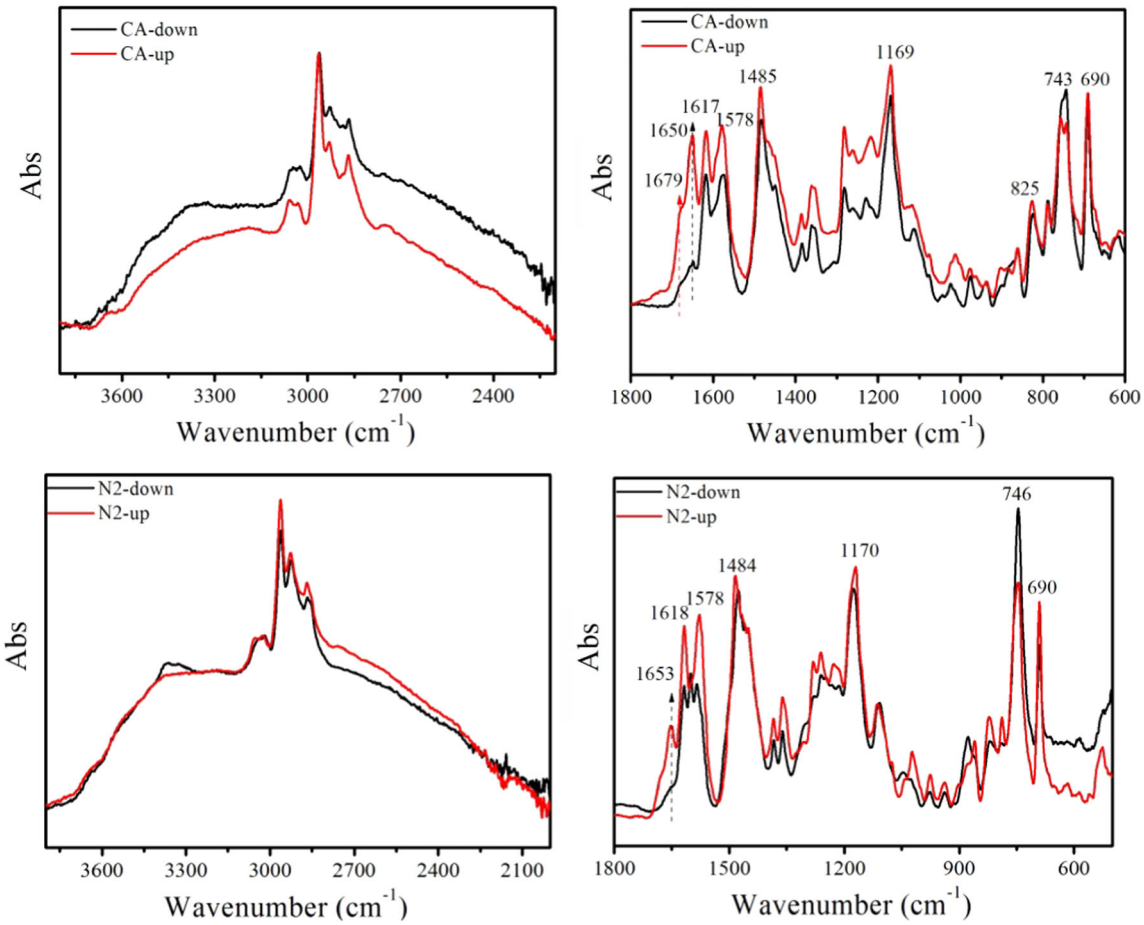

Figure 8 ATR-IR spectra of upper and lower surfaces of CA and N2.

Table 5 Hydrogen bonding distributions of the upper and lower surfaces of polybenzoxazine films from curve fitting of ATR-IR spectra in the range of 3800–1700 cm^{-1}

Sample	–O···H^+N^- (%)	–OH···N (%)	–OH···O (%)	–OH···π (%)	Intra-HB (%)
SA-up	49.0	28.0	15.7	7.3	77.0
SA-down	45.9	26.8	18.6	8.7	72.7
CA-up	43.5	30.2	19.0	7.3	73.7
CA-down	49.5	24.1	18.0	8.3	73.6
N2-up	48.6	26.2	16.2	9.0	74.8
N2-down	42.9	27.5	20.5	9.1	70.4
VA-up	50.7	25.4	14.3	9.6	76.1
VA-down	42.4	27.7	19.1	10.8	70.1

OH···N and –O···H^+N^-) hydrogen bonding. Consequently, the films cured in air were dark in color, brittle, possessed lower T_{d5} and T_g but higher Y_c. The investigation on the two surfaces of the films verified that upper surfaces were more inclined to decompose and form more intramolecular hydrogen bonding, thus showed bigger WCAs. On the basis of these findings, it is believed the structures and properties of polybenzoxazines can be well tuned by varying curing conditions.

Table 6 Water contact angles of the upper and lower surfaces of polybenzoxazine films

Sample	WCA (°)	WCA difference (°)
SA-up	57.0	5.2
SA-down	51.8	
CA-up	60.0	1.3
CA-down	58.7	
N2-up	62.4	6.8
N2-down	55.6	
VA-up	58.7	8.9
VA-down	49.8	

Acknowledgements

This work is supported by the National Natural Science Foundation of China (Project no. 21104048).

Compliance with ethical standards

Conflict of interest The authors declare no competing financial interest.

Electronic supplementary material: The online version of this article (https://doi.org/10.1007/s10853-020-05425-5) contains supplementary material, which is available to authorized users.

References

[1] Ning X, Ishida H (1994) Phenolic materials via ring-opening polymerization: synthesis and characterization of Bisphenol A based benzoxazine and their polymers. J Polym Sci Part A Polym Chem 32(6):1121–1129

[2] Ishida H, Krus CM (1998) Synthesis and characterization of structurally uniform model oligomers of polybenzoxazine. Macromolecules 31(8):2409–2418

[3] Shen SB, Ishida H (1999) Dynamic mechanical and thermal characterization of high-performance polybenzoxazines. J Polym Sci Part B 37(23):3257–3268

[4] Agag T, Jin L, Ishida H (2009) A new synthetic approach for difficult benzoxazines: preparation and polymerization of 4,4′-diaminodiphenyl sulfone-based benzoxazine monomer. Polymer 50(25):5940–5944

[5] Dogan Demir K, Kiskan B, Yagci Y (2011) Thermally curable acetylene-containing main-chain benzoxazine polymers via sonogashira coupling reaction. Macromolecules 44(7):1801–1807.

[6] Ran QC, Yi G (2015) Concerted reactions of aldehyde groups during polymerization of an aldehyde-functional benzoxazine. J Polym Sci Part A Polym Chem 49(7):1671–1677

[7] Šebenik U, Krajnc M (2015) Synthesis, curing kinetics, thermal and mechanical behavior of novel cardanol-based benzoxazines. Polymer 76:203–212

[8] Zhang S, Yang P, Bai Y, Zhou T, Zhu R, Gu Y (2017) Polybenzoxazines: thermal responsiveness of hydrogen bonds and application as latent curing agents for thermosetting resins. ACS Omega 2(4):1529–1534

[9] Ghosh NN, Kiskan B, Yagci Y (2007) Polybenzoxazines—new high performance thermosetting resins: synthesis and properties. Prog Polym Sci 32(11):1344–1391

[10] Nair CPR (2004) Advances in addition-cure phenolic resins. Prog Polym Sci 29(5):401–498

[11] Kiskan B (2018) Adapting benzoxazine chemistry for unconventional applications. React Funct Polym 129:76–88

[12] Chou CI, Liu YL (2010) High performance thermosets from a curable Diels–Alder polymer possessing benzoxazine groups in the main chain. J Polym Sci Part A Polym Chem 46(19):6509–6517

[13] He X-Y, Wang J, Wang Y-D, Liu C-J, Liu W-B, Yang L (2013) Synthesis, thermal properties and curing kinetics of fluorene diamine-based benzoxazine containing ester groups. Eur Polym J 49(9):2759–2768

[14] Dumas L, Bonnaud L, Olivier M, Poorteman M, Dubois P (2016) High performance bio-based benzoxazine networks from resorcinol and hydroquinone. Eur Polym J 75:486–494

[15] Zhang K, Yu X (2018) Catalyst-free and low-temperature terpolymerization in a single-component benzoxazine resin containing both norbornene and acetylene functionalities. Macromolecules 51(16):6524–6533

[16] Su YC, Chang FC (2003) Synthesis and characterization of fluorinated polybenzoxazine material with low dielectric constant. Polymer 44(26):7989–7996

[17] Su Y-C, Chen W-C, Ou K-L, Chang F-C (2005) Study of the morphologies and dielectric constants of nanoporous materials derived from benzoxazine-terminated poly(ε-caprolactone)/polybenzoxazine co-polymers. Polymer 46(11):3758–3766

[18] Lin CH, Huang SJ, Wang PJ, Lin HT, Dai SA (2012) Miscibility, microstructure, and thermal and dielectric properties of reactive blends of dicyanate ester and diamine-based benzoxazine. Macromolecules 45(18):7461–7466

[19] Zhang S, Yan Y, Li X, Fan H, Ran Q, Fu Q, Gu Y (2018) A novel ultra low-k nanocomposites of benzoxazinyl modified polyhedral oligomeric silsesquioxane and cyanate ester. Eur Polym J 103:124–132

[20] Kobzar YL, Tkachenko IM, Lobko EV, Shekera OV, Syrovets AP, Shevchenko VV (2017) Low dielectric material from novel core-fluorinated polybenzoxazine. Mendeleev Commun 27(1):41–43

[21] Ilango K, Prabunathan P, Satheeshkumar E, Manohar P (2017) Design of low dielectric constant polybenzoxazine nanocomposite using mesoporous mullite. High Perform Polym 29(2):141–150

[22] Rimdusit S, Lohwerathama M, Hemvichian K, Kasemsiri P, Dueramae I (2013) Shape memory polymers from benzoxazine-modified epoxy. Smart Mater Struct 22(7):075033

[23] Zhang S, Ran Q, Fu Q, Gu Y (2018) Preparation of transparent and flexible shape memory polybenzoxazine film through chemical structure manipulation and hydrogen bonding control. Macromolecules 51(17):6561–6570

[24] Taskin OS, Kiskan B, Yagci Y (2013) Polybenzoxazine precursors as self-healing agents for polysulfones. Macromolecules 46(22):8773–8778

[25] Sharma P, Shukla S, Lochab B, Kumar D, Kumar Roy P (2014) Microencapsulated cardanol derived benzoxazines for self-healing applications. Mater Lett 133:266–268

[26] Wan L, Wang J, Xie L, Sun Y, Li K (2014) Nitrogen-enriched hierarchically porous carbons prepared from polybenzoxazine for high-performance supercapacitors. ACS Appl Mater Interfaces 6(17):15583–15596

[27] Alhwaige AA, Ishida H, Qutubuddin S (2016) Carbon aerogels with excellent CO2 adsorption capacity synthesized from clay-reinforced biobased chitosan-polybenzoxazine nanocomposites. ACS Sustain Chem Eng 4(3):1286–1295

[28] Wu J-Y, Mohamed MG, Kuo S-W (2017) Directly synthesized nitrogen-doped microporous carbons from polybenzoxazine resins for carbon dioxide capture. Polym Chem 8(36):5481–5489

[29] Wang C, Sun J, Liu X, Sudo A, Endo T (2012) Synthesis and copolymerization of fully bio-based benzoxazines from guaiacol, furfurylamine and stearylamine. Green Chem 14(10):2799–2806

[30] Rao BS, Palanisamy A (2011) Monofunctional benzoxazine from cardanol for bio-composite applications. React Funct Polym 71(2):148–154

[31] Lligadas G, Tüzün A, Ronda JC, Galià M, Cádiz V (2014) Polybenzoxazines: new players in the bio-based polymer arena. Polym Chem 5(23):6636–6644

[32] Zhang K, Han M, Liu Y, Froimowicz P (2019) Design and synthesis of bio-based high-performance trioxazine benzoxazine resin via natural renewable resources. ACS Sustain Chem Eng 7(10):9399–9407

[33] Zhang L, Yang Y, Chen Y, Lu H (2017) Cardanol-capped main-chain benzoxazine oligomers for resin transfer molding. Eur Polym J 93:284–293

[34] Plengudomkit R, Okhawilai M, Rimdusit S (2016) Highly filled graphene-benzoxazine composites as bipolar plates in fuel cell applications. Polym Compos 37(6):1715–1727

[35] Patil DM, Phalak GA, Mhaske S (2017) Enhancement of anti-corrosive performances of cardanol based amine functional benzoxazine resin by copolymerizing with epoxy resins. Prog Org Coat 105:18–28

[36] Renaud A, Poorteman M, Escobar J, Dumas L, Bonnaud L, Dubois P, Olivier M-G (2017) A new corrosion protection approach for aeronautical applications combining a PhenolparaPhenyleneDiAmine benzoxazine resin applied on sulfotartaric anodized aluminum. Prog Org Coat 112:278–287

[37] Wang YX, Ishida H (1999) Cationic ring-opening polymerization of benzoxazines. Polymer 40(16):4563–4570

[38] Chutayothin P, Ishida H (2010) Cationic ring-opening polymerization of 1,3-benzoxazines: mechanistic study using model compounds. Macromolecules 43(10):4562–4572

[39] Wang YX, Ishida H (2000) Synthesis and properties of new thermoplastic polymers from substituted 3,4-dihydro-2h-1,3-benzoxazines. Macromolecules 33(8):2839–2847

[40] Wang MW, Jeng RJ, Lin CH (2015) Study on the ring-opening polymerization of benzoxazine through multisubstituted polybenzoxazine precursors. Macromolecules 48(3):530–535

[41] Ishida H, Sanders DP (2000a) Regioselectivity and network structure of difunctional alkyl-substituted aromatic amine-based polybenzoxazines. Macromolecules 33(22):8149–8157

[42] Sudo A, Kudoh R, Nakayama H, Arima K, Endo T (2008) Selective formation of poly(N, O-acetal) by polymerization of 1,3-benzoxazine and its main chain rearrangement. Macromolecules 41(23):9030–9034

[43] Ran Q-C, Zhang D-X, Zhu R-Q, Gu Y (2012a) The structural transformation during polymerization of benzoxazine/FeCl3 and the effect on the thermal stability. Polymer 53(19):4119–4127

[44] Chao L, Shen D, SebastiáN RMA, Marquet J, SchöNfeld R (2011) Mechanistic studies on ring-opening polymerization of benzoxazines: a mechanistically based catalyst design. Macromolecules 44(12):4616–4622

[45] Zhang S, Ran Q, Fu Q, Gu Y (2019a) Controlled polymerization of 3,4-dihydro-2H-1,3-benzoxazine and its properties tailored by Lewis acids. React Funct Polym 139:75–84

[46] Zhang S, Ran Q, Fu Q, Gu Y (2019b) Thermal responsiveness of hydrogen bonding and dielectric property of polybenzoxazines with different Mannich bridge structures. Polymer 175:302–309

[47] Han L, Salum ML, Zhang K, Froimowicz P, Ishida H (2017) Intrinsic self-initiating thermal ring-opening polymerization of 1,3-benzoxazines without the influence of impurities

using very high purity crystals. J Polym Sci Part A Polym Chem 55(20):3434–3445
[48] Macko J, Ishida H (2000) Behavior of a bisphenol-A-based polybenzoxazine exposed to ultraviolet radiation. J Polym Sci Part B Polym Phys 38:2687–2701
[49] Ishida H, Hong YL (1997) A study on the volumetric expansion of benzoxazine-based phenolic resin. Macromolecules 30(4):1099–1106
[50] Kim H-D, Ishida H (2002) A study on hydrogen-bonded network structure of polybenzoxazines. J Phys Chem A 106(14):3271–3280
[51] Yang P, Wang X, Fan H, Gu Y (2013) Effect of hydrogen bonds on the modulus of bulk polybenzoxazines in the glassy state. Phys Chem Chem Phys 15(37):15333–15338
[52] Wirasate S, Dhumrongvaraporn S, Allen DJ, Ishida H (2015) Molecular origin of unusual physical and mechanical properties in novel phenolic materials based on benzoxazine chemistry. J Appl Polym Sci 70(7):1299–1306
[53] Bai Y, Yang P, Song Y, Zhu R, Gu Y (2016) Effect of hydrogen bonds on the polymerization of benzoxazines: influence and control. RSC Adv 6(51):45630–45635
[54] Wang B, Yang P, Li Y, He Y, Zhu R, Gu Y (2017) Blends of polybenzoxazine/poly (acrylic acid): hydrogen bonds and enhanced performances. Polym Int 66:1159–1163
[55] Su Y-C, Kuo S-W, Yei D-R, Xu H, Chang F-C (2003) Thermal properties and hydrogen bonding in polymer blend of polybenzoxazine/poly (N-vinyl-2-pyrrolidone). Polymer 44(8):2187–2191
[56] Li X, Yi G (2011) The co-curing process of a benzoxazine-cyanate system and the thermal properties of the copolymers. Polym Chem 2(12):2778–2781
[57] Zhuang Y, Gu Y (2013) Poly(benzoxazole-amide-imide) copolymers for interlevel dielectrics: interchain hydrogen bonding, molecular arrangement and properties. J Polym Res 20(6):1–8
[58] Wang X, Zong L, Han J, Wang J, Liu C, Jian X (2017) Toughening and reinforcing of benzoxazine resins using a new hyperbranched polyether epoxy as a non-phase-separation modifier. Polymer 121:217–227
[59] Liu Y, Gao S, Gong X, Xue Q, Lu Z (2019) Benzoxazine-epoxy thermosets with smectic phase structures for high thermal conductive materials. Liquid Cryst 46:1–10
[60] Zeng K, Huang J, Ren J, Ran Q (2019) Curing reaction of benzoxazine under high pressure and the effect on thermal resistance of polybenzoxazine. Macromol Chem Phys 220(1):1800340
[61] Ran Q-C, Zhang D-X, Zhu R-Q, Gu Y (2012b) The structural transformation during polymerization of benzoxazine/FeCl 3 and the effect on the thermal stability. Polymer 53(19):4119–4127
[62] Liu Y, Wang R, An Q, Su X, Li C, Shen S, Huo G (2017) The F··· H hydrogen bonding effect on the dynamic mechanical and shape-memory properties of a fluorine-containing polybenzoxazine. Macromol Chem Phys 218(15):1700079
[63] Lin CH, Chang SL, Shen TY, Shih YS, Lin HT, Wang CF (2012) Flexible polybenzoxazine thermosets with high glass transition temperatures and low surface free energies. Polym Chem 3(4):935–945
[64] Treloar RGL (1958) The physics of rubber elasticity. 2nd ed, The Clarendon Press
[65] Ishida H, Allen DJ (1996) Mechanical characterization of copolymers based on benzoxazine and epoxy. Polymer 37(20):4487–4495
[66] Ishida H, Sanders DP (2000b) Improved thermal and mechanical properties of polybenzoxazines based on alkyl-substituted aromatic amines. J Polym Sci Part B Polym Phys 38(24):3289–3301
[67] Laobuthee A, Chirachanchai S, Ishida H, Tashiro K (2001) Asymmetric mono-oxazine: an inevitable product from Mannich reaction of benzoxazine dimers. J Am Chem Soc 123(41):9947–9955
[68] Chirachanchai S, Laobuthee A, Phongtamrug S (2009) Self termination of ring opening reaction of p-substituted phenol-based benzoxazines: an obstructive effect via intramolecular hydrogen bond. J Heterocycl Chem 46(4):714–721
[69] Bai Y, Yang P, Wang T, Gu Y (2017) Hydrogen bonds in the blends of polybenzoxazines and N, N′-(pyridine-2, 6-diyl) diacetamide: Inter-or intra-molecular hydrogen bonds? J Mol Struct 1147:26–32
[70] Alhwaige AA, Ishida H, Qutubuddin S (2019) Poly(benzoxazine-f-chitosan) films: the role of aldehyde neighboring groups on chemical interaction of benzoxazine precursors with chitosan. Carbohydr Polym 209:122–129
[71] Chih-Feng W, Yi-Ting W, Pao-Hsiang T, Shiao-Wei K, Chun-Hung L, Yuung-Ching S, Feng-Chih C (2006) Stable superhydrophobic polybenzoxazine surfaces over a wide pH range. Langmuir ACS J Surf Colloids 22(20):8289–8292
[72] Chih-Feng W, Yi-Che S, Shiao-Wie K, Chih-Feng H, Yuung-Ching S, Feng-Chih C (2010) Low-surface-free-energy materials based on polybenzoxazines. Angew Chem Int Ed 45(14):2248–2251